Contents list available at CBIORE journal website

International Journal of Renewable Energy Development

Journal homepage: https://ijred.cbiore.id

Research Article

Evaluation of the effects of fatty ester isomerization and turpentine-derived additive introduction on biodiesel cold flow properties and oxidation stability

Antonius Indarto[a,b*], Yano Surya Pradana[c,d], Alif Kembara Alam[e], I Gusti Bagus Ngurah Makertihartha[a], Tirto Prakoso[a], Tatang Hernas Soerawidjaja[b]

[a]*Department of Chemical Engineering, Faculty of Industrial Technology, Institut Teknologi Bandung, Bandung, Indonesia*

[b]*Department of Bioenergy Engineering and Chemurgy, Faculty of Industrial Technology, Institut Teknologi Bandung, Sumedang, Indonesia*

[c]*Doctoral Program of Chemical Engineering, Faculty of Industrial Technology, Institut Teknologi Bandung, Bandung, Indonesia*

[d]*Department of Chemical Engineering, Faculty of Engineering, Universitas Gadjah Mada, Yogyakarta, Indonesia*

[e]*Master Program of Chemical Engineering, Faculty of Industrial Technology, Institut Teknologi Bandung, Bandung, Indonesia*

Abstract. Biodiesel is a cleaner and renewable combustion fuel that globally serves as an effective alternative to fossil diesel. The current application of this biofuel is still restricted to specific concentration due to its poor cold flow properties (CFPs) and low oxidation stability (OS). Later, isomerization process was offered to improve cold flow properties as well as oxidation stability. In this study, palm-biodiesel isomerization was carried out atmospherically using SO_4/SnO_2 catalyst, prepared via wet nitration method, in the stirred batch reactor at temperature of 200°C, catalyst loading of 10 wt%, stirring speed of 900 rpm, and under N_2 flow. The performance of catalyst and the effect of fatty ester isomerization on CFPs and OS were investigated. For comparative study, the effect of bio-additive (turpentine oil and α-terpineol) introduction, at concentrations of 1−10 vol%, on CFPs and OS was also evaluated. The isomerization results demonstrated a conversion ratio of 12.54±0.60%, an isomerization selectivity of 75.92±5.79%, and an overall turnover frequency of $1.75\times10^{-1}\pm8.5\times10^{-3}$ h^{-1}. This reaction had a small reduction in pour point (ΔPP = –1°C), a minor elevation in cloud point (ΔCP = 0.50±0.15°C), and a slight improving effect in OS (ΔOS = 1.36 h). Furthermore, the optimum insertion of bio-additive was α-terpineol at concentration of 5 vol%, demonstrating a more significant enhancement in CFP parameters (ΔPP = –1°C; ΔCP = –1.75±0.15°C). Nevertheless, it significantly reduced OS level (ΔOS = –11 h), although the absolute value (OS = 10.36 h) remains compliant with international standards.

Keywords: Biodiesel, cold flow properties, oxidation stability, isomerization, SO_4/SnO_2 catalyst, bio-additive

Received: 7th Nov 2025; Revised: 6th January 2026; Accepted: 8th February 2026; Available online: 20th February 2026

1. Introduction

Humans fundamentally require energy to accomplish various tasks. Interestingly, the demand for energy persistently escalates each year, both in type and quantity, reflecting ongoing diversification and growth in consumption patterns (Pan *et al*., 2022). Energy diversification is primarily influenced by the rapid shifts in lifestyle, environmental concerns, and advancements in technology (Dey *et al*., 2021). Then, the massive elevation in energy quantity is driven by the accelerating increase in human population (Leng *et al*., 2020). However, the expansion of energy demand is needed to encourage regional economic growth, with a strong positive correlation (László, 2023). The more energy supply supports the enhancement in production, consumption, and transportation activities (Pradana *et al*., 2018; Prasakti *et al*., 2020).

Nonetheless, current energy sources are insufficient to meet this rising request (Yuarrina *et al*., 2018). The availability of fossil-based fuels as principal energy is diminishing annually, leading to energy shortages and elevated costs (Riyadi *et al*., 2023). Additionally, the excessive use of fossil fuels should be avoided to minimize environmental and health risks associated with emissions (Pradana *et al*., 2021; Wahyono *et al*., 2020). To address those challenges, all stakeholders are actively working to produce renewable and cleaner energy sources. Among these options, biodiesel is considered a viable preference (Lugito *et al*., 2025).

Biodiesel, a sustainable substitute for fossil diesel, is generally manufactured through chemical reactions involving fatty acids and alcohols with the involvement of catalyst, yielding fatty esters (Pradana *et al*., 2025a). Sources of fatty acids can be obtained from commercial edible oils (such as palm, soybean, and repeseed oils) and non-edible feedstocks (including Jatropha, rubber-seed, karanja, and waste oils) (L. Wang *et al*., 2023). Non-edible feedstocks are promoted to support or substitute edible oils as raw materials at a more affordable cost (Pradana *et al*., 2020). Moreover, the utilization

* Corresponding author
Email: antonius.indarto@itb.ac.id (A. Indarto)

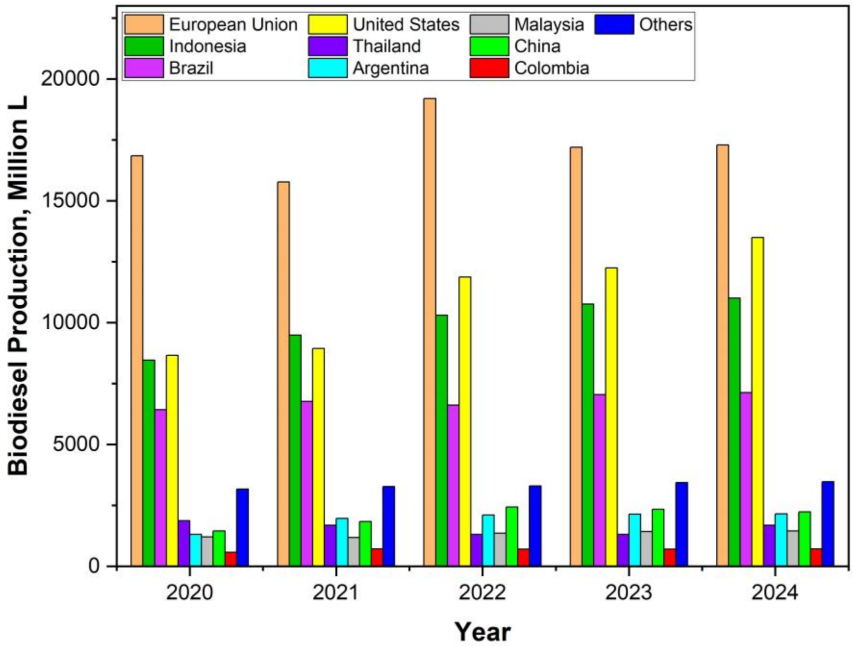

Fig. 1. Country or region-based biodiesel production in the recent five years. These data were collected from OECD & FAO (2024a).

of non-edible feedstocks also offers multiple benefits, such as diversification of raw material sources, mitigation of conflicts with the food industry, and contributions toward waste reduction (Jhoni & Pradana, 2025; Suzihaque *et al.*, 2022; Thushari *et al.*, 2019). Subsequently, the alcohols usually used as reactants are methanol and ethanol. However, alcohols with carbon chains of up to eight atoms, whether straight or branched, can also be utilized as reactants for certain purposes (Sierra-Cantor & Guerrero-Fajardo, 2017).

Over the past five years, global biodiesel production has shown consistent growth in volume. Based on data released by Organisation for Economic Co-operation and Development (OECD) in collaboration with Food and Agriculture Organization (FAO), in the period of 2020–2024, total production expanded from 49.9 billion liters to more than 60 billion liters (OECD & FAO, 2024b). This production volume is spread accross various countries and regions in the world, as depicted in Fig. 1. The most superior country or region for biodiesel manufacturing is European Union with total volume of 17.3 billion liters in 2024. The next three leading countries in biodiesel production are United States (13.5 billion liters), Indonesia (11 billion liters), and Brazil (7.1 billion liters). These countries have seen significant expansion in biodiesel production in the last five years to encourage their energy transition efforts. The combined production of these four dominant countries or regions is 48.9 billion liters or over 80% of world production. Of this amount, vegetable oils-based biodiesel was still the mainstay with a dominance of 70% (OECD & FAO, 2024a). Most recently, used cooking oils have also attracted the attention of several producers as plentiful and cost-effective feedstocks (OECD & FAO, 2024b).

Although biodiesel demonstrates promising potential, its implementation in regular diesel engines faces several challenges. The elevated proportion of saturated fatty esters adversely affects cold fluidity (Amran *et al.*, 2022; Santos *et al.*, 2023). Poor cold fluidity allows for clogging of fuel flow lane at low ambient temperature (Sia *et al.*, 2020). Nevertheless, improving this property by increasing unsaturation in the fatty ester chains, as presented in Fig. 2, worsens oxidation stability. It technically diminishes fuel calory, corrodes engine parts faster, and releases higher emission (Anwar & Garforth, 2016; Lanjekar & Deshmukh, 2016). Then, isomerization process is proposed to refine cold flow properties and oxidation stability.

Isomerization is a chemical process that alters the arrangement of atoms within a compound without changing its overall chemical formula (Pradana *et al.*, 2024). Isomerization can be divided into five categories, but this study focuses on skeletal (branching) and geometric (*cis-trans*) isomerization. The first mentioned category directly promotes better biodiesel fluidity at low temperature, while the second improves stability against oxidation (Anwar & Garforth, 2016). Basically, *cis-trans* isomerization reaction necessitates an acid catalyst to lessen the activation energy, facilitating the process (Liu *et al.*, 2019; Misra *et al.*, 2023). Among several types of acid catalysts, solid superacid catalysts have emerged as prominent isomerization catalysts due to their excellence in acidity and solid form (Sierra-Cantor & Guerrero-Fajardo, 2017; Varala *et al.*, 2016). According to Arata *et al.* (2003), sulfated tin(IV) oxide (SO_4/SnO_2) was recognized as the most acidic metal oxide. Because of this characteristic, SO_4/SnO_2 material is expected to exhibit notable catalytic activity in isomerization reaction.

Thereafter, this research was conducted to examine the characteristics and activity of SO_4/SnO_2 catalyst in the biodiesel isomerization. This catalyst was synthesized via wet nitration method, in which tin metal was reacted with nitric acid to generate meta-stannic acid. Subsequently, the meta-stannic acid was modified using sulfate anions. This technique differs from the hydrolysis approach previously studied (Pradana *et al.*, 2025b). According to Hino et al. (2007), SO_4/SnO_2 catalysts derived from meta-stannic acid exhibited superior catalytic activity compared to those prepared via hydrolysis of tin salts. This reaction was investigated with respect to its impact on biodiesel cold flow behavior and oxidation stability.

In addition, this research also examined the insertion of terpentine oil and α-terpineol as biodiesel cold flow modifiers. Turpentine oil has been reported to enhance the cold fluidity of B40 (Achmad *et al.*, 2025) and blended B100 (Ballesteros *et al.*, 2020). Meanwhile, the influence of α-terpineol on biodiesel cold flow properties has not been extensively studied. Then, this investigation was conducted to observe their influence on biodiesel low-temperature operability and oxidative resistance,

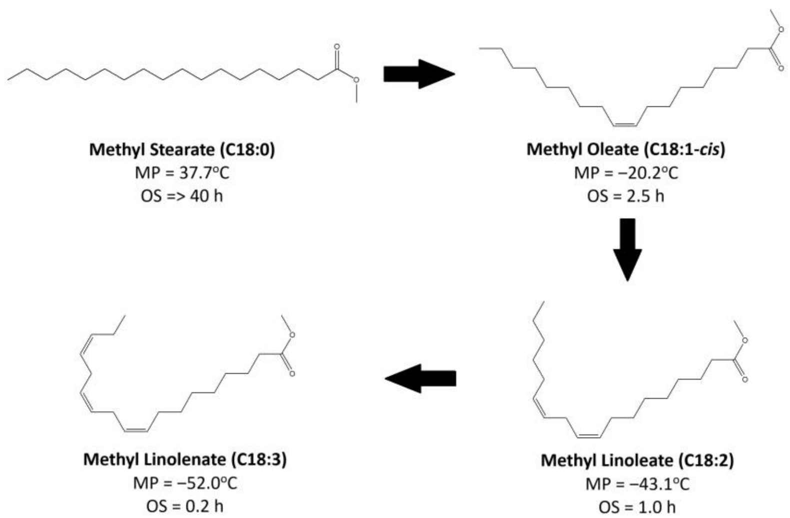

Fig. 2. Effect of unsaturation process on melting point and oxidation stability of C-18 fatty esters. These data were collected from Anwar & Garforth (2016), Moser (2009), and Knothe & Dunn (2009)**.**

comparing the results with those obtained through isomerization.

2. Materials and Methods

2.1 Materials

This investigation utilized several essential materials for catalyst production, including tin powder ≥99.5% (Sigma Aldrich, USA), HNO_3 solution ≥65% (Merck, Germany), H_2SO_4 solution 95–97% (Merck, Germany), and diphenylamine (Sigma Aldrich, USA). For catalyst acidity test, sodium hydroxide (NaOH) pellets ≥99% and halite (NaCl) ≥99.5% were purchased from Merck, Germany. For reaction, palm biodiesel consisting of fatty acid methyl esters was provided by PT Sinarmas Bio Energy (Indonesia) in two delivery batches. Subsequently, n-hexane ≥99%, supplied by Merck (Germany), was utilized as solvent for sample preparation of biodiesel feedstock and isomerization product. Meanwhile, turpentine oil and α-terpineol (≥97%) as bio-additives were obtained from Perhutani Pine Chemical Industry (Pemalang, Indonesia).

2.2 Catalyst Preparation

In this study, STO catalyst was manufactured via two-step technique: (1) tin (IV) oxide (TO) synthesis through wet nitration process (Wenxiang *et al.*, 2005); and (2) sulfate promotion on TO materials. In the first step, TO was prepared by reacting high purity tin metal with concentrated nitric acid at Sn–HNO_3 weight ratio of 1:8 and temperature range of 85–90°C. The sediment was then rinsed with distilled water to ensure complete removal of nitrates. The absence of nitrate ion footprints was determined by introducing diphenylamine reagent, which was dissolved in sulfuric acid, into the washing wastewater till the solution ceased to exhibit a blue color. Subsequently, the nitrate-free TO solids were oven-dried overnight at 105°C. For second step, the dry TO solids were sulfated with excess 3M sulfuric acid for 1 h and the sulfated TO was oven-dried at 105°C for 2 h. Later, the pristine and sulfate-modified TO materials were calcined at 500°C for 3 h.

2.3 Catalyst Characterization

The produced STO catalyst underwent examination to determine its thermal stability properties at temperature span of 30–1000°C, atmospheric pressure, and heating rate of 10°C/min. This characterization was carried out using Simultaneous Thermal Analysis Instrument (Model PT-1600) manufactured by Linseis Inc. Then, the crystalline structures of calcined TO and STO materials were characterized using X-ray Powder Diffraction Analyzer (Type D2 Phaser) fabricated by Bruker Corporation. The X-ray, operated in this diffractometer, was generated from Cu-Kα radiation at wavelength of 1.5406 Å. Additionally, the diffraction angles (2θ) used for crystal scanning were in the range of 10–80 degrees.

The functional groups of calcined TO and STO solids were identified using Fourier Transform Infra-red (FT-IR) spectra provided by Bruker Alpha Infra-Red Spectrometer equipped with Platinum-Attenuated Total Reflectance. In this study, the infra-red transmittance was observed at wavelength between 500-2000 cm^{-1}. Next, the composition of elements and chemical compounds for calcined TO and STO materials was evaluated using X-ray Fluorescence Spectrometer (Type NEX-CG) engineered by Rigaku Holdings Corporation. For nitrogen-sorption, BET analysis was isothermally conducted at 195.8°C using Tristar II Plus Analyzer fabricated by Micromeritics Instrument Corporation.

Afterwards, *Bronsted* acidity test for calcined TO and STO solids was performed via potentiometric titration technique. In this method, a certain weight of NaOH pellets was inserted into 4% NaCl solution to provide 0.05M sodium hydroxide solution as a titrant. Later, this titrant was gradually dripped onto the catalyst suspension (1.0 g STO in 100 ml 4% NaCl solution). The pH of the catalyst suspension was measured for every 0.5 ml drop of titrant, until it reached 10. Then, the acid concentration was specifically quantified based on the titration data (Yu *et al.*, 2016).

2.4 Catalyst Activity Test

The isomerization experiment was carried out over STO catalyst, with two replications, in the stirred batch reactor. The feed was palm biodiesel from the first delivery batch. The operating conditions were set at ambient pressure, catalyst percentage of 10 wt%, mixing speed of 900 rpm, and residence period of 12 h. The reaction temperature was also optimized at 200°C to minimize potential carbon-chain cracking at higher temperatures and prevent a decrease in catalyst activity at lower temperatures. Once the reaction was complete, the biodiesel product was filtered to segregate it from the spent catalyst.

Hereinafter, the components and composition of biodiesel (feedstock and product) were scanned utilizing gas chromatography-mass spectrometry (GC-MS). This equipment set, consisting of Claurus 600 Gas Chromatograph and Claurus 600T Mass Spectrometer, was fabricated by PerkinElmer, Inc. The GC packed column used for biodiesel sample was Perkin Elmer Elite-5ms Column with an inside diameter of 0.25 mm and a length of 30 m. In this investigation, helium, used as the inert gas, was employed at a split value of 90:1. The initial and final temperatures were assigned at 180 and 260°C, respectively, with a ramp of 5°C/min. The GC-MS results were then utilized to calculate overall conversion ratio (CR), product yield (Y), and selectivity (S) using Eq. (1) – (3). In these equations, $m_{i,B}$ and $m_{i,A}$ referred to the weight of reactant component "i" before and after reaction, respectively. Meanwhile, $m_{j,z,A}$ and $m_{j,z,B}$ denoted the weight of product component "j", related to process "z", following and preceding the reaction, respectively.

$$CR\ (\%) = \frac{\sum(m_{i,B}-m_{i,A})}{\sum m_{i,B}} x\ 100\% \quad (1)$$

$$Y_z\ (\%) = \frac{\sum(m_{j,z,A}-m_{j,z,B})}{\sum m_{i,B}} x\ 100\% \quad (2)$$

$$S_z\ (\%) = \frac{\sum(m_{j,z,A}-m_{j,z,B})}{\sum(m_{i,B}-m_{i,A})} x\ 100\% \quad (3)$$

Additionally, the catalytic activity associated with *Bronsted* acid sites was quantified using turnover frequency (TOF) parameter. The TOF calculation was conducted using formula presented in Eq. (4). $N_{i,B}$ and $N_{i,A}$ symbolized the mole of reactant component "i" before and after reaction, respectively. Next, m_{cat} and t_{react} pointed the mass of catalyst and the reaction time. Meanwhile, $A_{Bronsted}$ was *Bronsted* acidity measured using potentiometric titration method.

$$TOF\ (h^{-1}) = \frac{\sum(N_{i,B}-N_{i,A})}{m_{cat} \times A_{Bronsted} \times t_{react}} \quad (4)$$

2.5 Bio-additive introduction

For sample preparation, a bio-additive at certain percentages (1−10 vol%) was introduced into 20 ml biodiesel. At this stage, the biodiesel feedstock used in the experiments was obtained from the second delivery batch (Me-myristate = 0.3 wt%; Me-palmitate = 47.9 wt%; Me-stearate = 3.2 wt%; Me-oleate = 43.2 wt%; Me-linoleate = 5.4 wt%;). Each mixture was then stirred for 10 min to ensure homogeneity. After mixing, it was ready for cold flow properties and oxidation stability analysis.

2.6 Analysis of Cold Flow Properties and Oxidation Stability

The pour point (PP) and cloud point (CP) of biodiesel feedstocks and products were investigated using PCA-70Xi Analyzer provided by Phase Technology Company. This instrument was operated with the standards of ASTM D5949 and D5773 for PP and CP observation, respectively. Finally, the best isomerization sample in each variable was observed for oxidation stability using ASTM D6751 method. This analysis was run on the Metrohm 873 Rancimat Analyzer (Metrohm Co., Switzerland) at a constant temperature of 110°C.

3. Results and Discussion

3.1 Catalyst Characteristics

3.1.1 Thermogravimetry-Differential Thermal Analysis

The stability analysis of STO catalyst against thermal is demonstrated through thermogravimetric-differential thermal analysis (TG-DTA) curves shown in Fig. 3. The curves displayed three endothermic peak points spread across three heating test areas: (1) 30–200°C with peak point of 78°C; (2) 200–450°C with peak point of 264°C; and (3) >450°C with peak point of 604°C. Totally, this thermal exposure reduced STO weight by 10.0%. The first area denoted the removal of physical and chemical water content with mass loss percentage of 2.7 wt%. Initially, the TGA curve exhibited the negative mass loss, indicating an increase in solid weight. This phenomenon was primary driven by the adsorption of ambient moisture onto STO solids (Alaya & Rabah, 2017; Pradana *et al.*, 2025b).

The second endothermic peak, appearing between 200 and 450°C, corresponded to the decipherment of leftover H_2SO_4 solution and the loss of volatile matter content on the STO surface (Hino *et al.*, 2007; Pradana *et al.*, 2025b). Due to these occurrences, the weight of STO solids was slightly reduced by 0.7 wt%. In this temperature range, the absence of exothermic peak signified that sulfate anions were uniformly dispersed over the solid exterior, potentially inhibiting the dehydroxylation of tin hydroxide gel into tin oxide (Alaya & Rabah, 2017; Khalaf *et al.*, 2011). Later, the last heating area (>450°C) elucidated the decomposition of surface-bonded sulfate at peak point of 604°C. This step contributed to the largest mass loss with a percentage of 6.6%. Typically, sulfate ion decomposes into a non-acidic form, which is subsequently released from the TO solid at elevated temperatures (Pradana *et al.*, 2025b). Thus, the reaction requiring STO catalyst with optimum acidity properties is recommended to be conducted at temperatures below 450°C.

3.1.2 X-ray Crystallography

The crystalline construction of calcined TO and STO materials is depicted in Fig. 4A. The Bragg peaks of pristine TO were detected at 26.6°, 33.8°, 37.9°, 38.9°, 51.8°, 54.6°, 61.8°, 64.7°, 65.8°, 71.2°, and 78.6°. These diffraction angles were corresponded to the planes of (110), (101), (200), (111), (211), (220), (002), (310), (112), (301), (202), and (321), respectively. According to standard No. 41-1445, the observed planes represented tetragonal-shape cassiterite tin oxide. The appearance of these peaks and planes was also identified in the

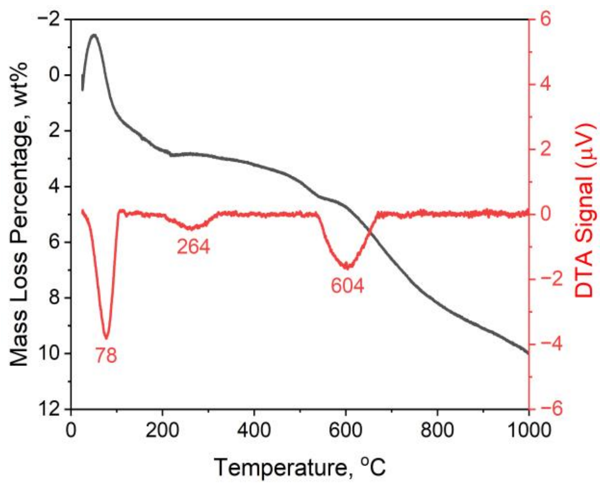

Fig. 3. TG-DTA curves of STO catalyst.

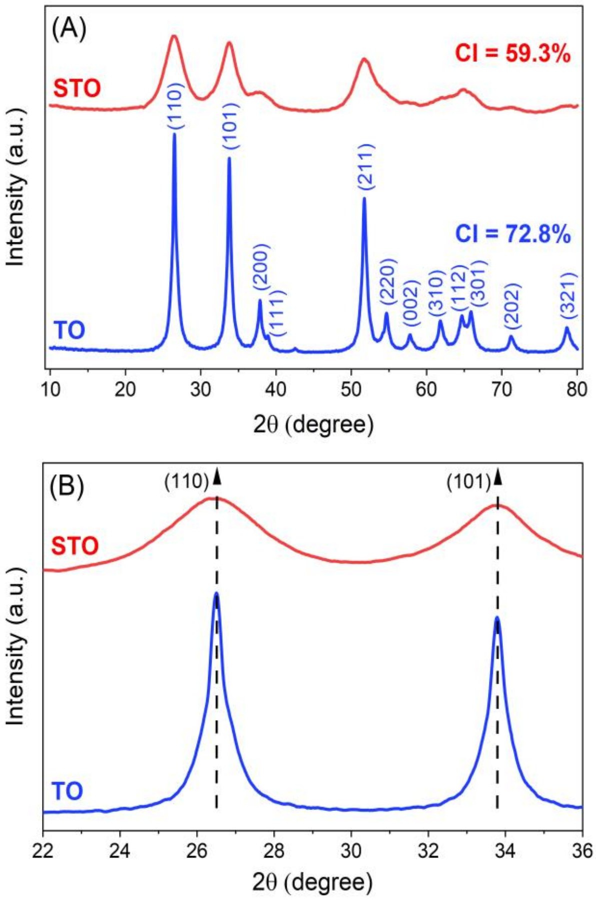

Fig. 4. (A) X-ray diffractograms and (B) peak shift analysis of TO and STO materials.

pure tin oxide prepared by Pradana *et al.* (2025b), Alaya & Rabah (2017), and Liu *et al.* (2019).

For STO material, the primary planes recognized in the diffractogram were (110), (101), (200), (211), and (112). The absence of sulfate peaks was due to the almost even spread of sulfate on the TO surface (Khalaf *et al.*, 2011). More details in Fig. 4B, sulfate modification also did not significantly shift the major tin oxide peaks (110) and (101). These results particularly indicated the similarity of tetragonal-lattice between TO and STO. Furthermore, the wider peaks in STO diffraction curve were due to the lower crystallinity index and smaller crystal dimension. It was proven by the lower crystallinity index of STO solid (59.3%) than TO material (72.8%). These results confirmed the hinderance of tin oxide crystal formation by sulfate anions (Alaya & Rabah, 2017).

3.1.3 Infra-red Vibrational Spectroscopy

In this analysis, TO and STO solids showed infra-red spectra as illustrated in Fig. 5. The vibration of Sn–O and O–Sn–O specifically appeared in the wavelength span of 500–700 cm^{-1}. These infra-red vibrations presented strong infra-red absorbances, asserting the prominent functional groups for both materials. The same situation was also presented in other results of TO-based materials (Alaya & Rabah, 2017; Liu *et al.*, 2019; Pradana *et al.*, 2025b).

Later, sulfate modification promoted the vibrations of Sn–OH, symmetrical S–O/S=O, asymmetrical S–O/S=O, and water component. These additional vibrations were respectively identified at wavelengths of 976, 1038, 1142, and 1636 cm^{-1}. The first mentioned vibration represented one of *Bronsted* acid groups contained in the STO solid (Akkera *et al.*, 2023). The second transmittance peak particularly indicated the existence of sulfate-based *Bronsted* acid on the solid exterior. Then, the asymmetrical S–O/S=O vibration denoted a non-acidic sulfate components in the form of bidentate sulfate complexes (Khalaf *et al.*, 2011). Lastly, the spectrum of 1636 cm^{-1} exhibited the existence of residual water in the prepared STO (Akkera *et al.*, 2023; Liu *et al.*, 2019).

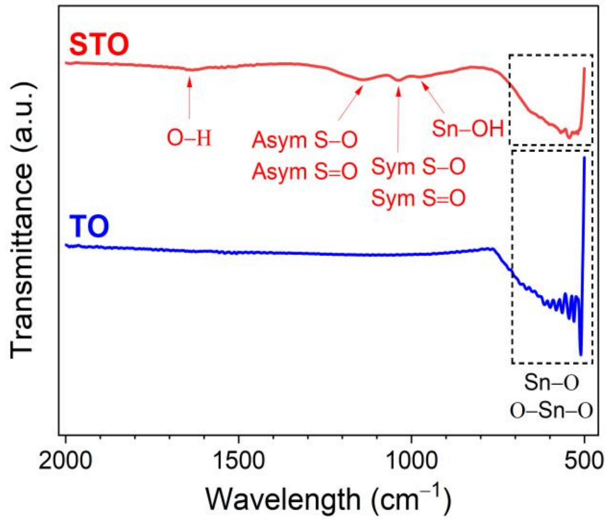

Fig. 5. FTIR spectra of TO and STO materials.

3.1.4 X-ray Fluorescence

The results of X-ray fluorescence for TO and STO materials are displayed in Table 1. Both materials were confirmed to predominantly contain tin metal in the form of tin(IV) oxide. The distinction was found in the absolute tin metal composition influenced by sulfation treatment. The promotion of sulfate anions into TO solids obviously elevated S and SO_3 content while declining Sn and SnO_2 levels. These compositions proved that sulfate anions were incorporated into TO solids. The similar effects of sulfate addition on SnO_2 and SO_3 content also occurred in previous study by Pradana *et al.*, 2025b.

3.1.5 Nitrogen Physisorption

Table 1
XRF-based chemical composition of TO and STO materials.

Component/element	Composition (wt%)	
	TO	STO
Oxide components:		
SnO_2	94.47	87.7
SO_3	0.06	7.77
CaO	2.84	2.12
Al_2O_3	0.28	0.19
K_2O	1.59	1.39
Elements:		
Sn	74.41	69.08
S	0.03	3.11
O	21.68	24.55
Ca	2.03	1.52
Al	0.15	0.10
K	1.32	1.15

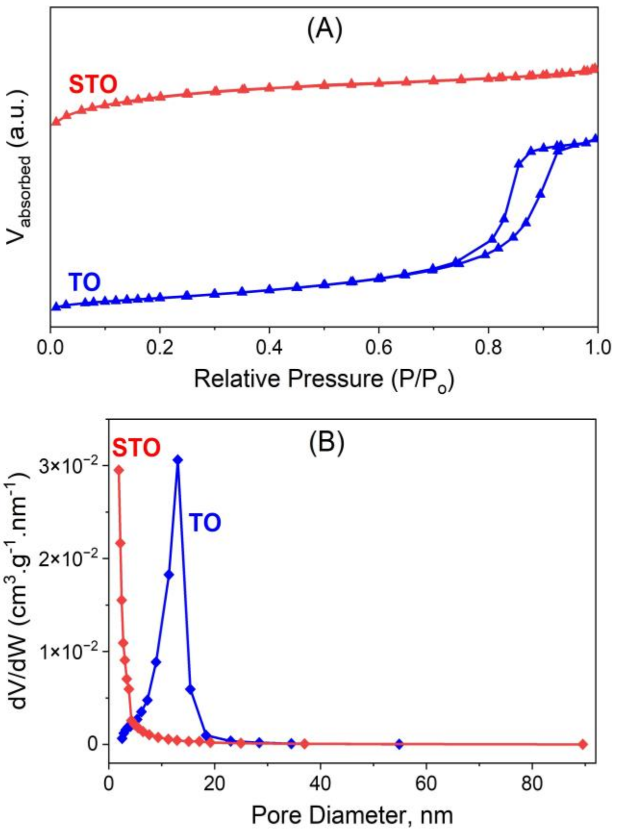

Fig. 6. (A) Nitrogen-sorption isotherm curves and (B) pore diameter distribution of TO and STO materials.

The results of nitrogen physical sorption and pore size distribution for TO and STO materials are demonstrated in Fig. 6. Based on Fig. 6A, TO isotherm curve was categorized as Type IV hysteresis curve with Type H2 loop, indicating a mesoporous texture (Thommes *et al.*, 2015). This investigation was supported by the pore size distribution curve (Fig. 6B), showing a peak level at a pore diameter of 13.03 nm. Then, according to Table 2, this material presented an average pore diameter of 14.5 nm with a total surface area of 43.5 $m^2.g^{-1}$. Additionally, total pore volume was observed at 0.16 $cm^3.g^{-1}$.

Hereafter, sulfate promotion transformed TO solids into microporous structure (Type I hysteresis curve) (Thommes *et al.*, 2015). It was due to the inhibition of crystallization as well as the coverage of pore surface by sulfate anions. From Fig. 6B, the pore size of STO material was concentrated at micropore and narrow mesopore diameters with a peak of 1.89 nm. The average pore size of STO solids, as indicated in Table 2, was measured at 3.2 nm. Technically, this pore size was eligible for the passage of fatty ester molecules. The largest size of fatty ester molecules was close to that of the stearic acid molecule at 2.45 x 0.25 nm (Anwar & Garforth, 2016). This point was crucial for facilitating the mass transfer of reacting molecules within the catalyst pores. The smaller pore size led to the higher surface area. Total surface and micropore areas were reported at 137.1 and 37.6 $m^2.g^{-1}$, respectively. Moreover, total pore volume decreased significantly, halving to 0.06 $cm^3.g^{-1}$.

Table 2
Solid textural properties of TO and STO materials.

Parameter	TO	STO
Total surface area ($m^2.g^{-1}$)	43.5	137.1
Micropore area ($m^2.g^{-1}$)	–	37.6
Total pore volume ($cm^3.g^{-1}$)	0.16	0.08
Average pore diameter (nm)	14.5	3.2

Furthermore, the quantitative results of solid surface analysis using BET method are tabulated in Table 2. The mean pore size of SnO_2 (14.6 nm) has been demonstrated to be larger than that of $Ni/SO_4/SnO_2$ (3.3 nm). In this situation, the smaller pore size of $Ni/SO_4/SnO_2$ solid is mainly due to the imperfect crystallization of tin(IV) hydroxide influenced by sulfate hindrance (Pradana *et al.*, 2025b). This pore size parameter proportionally correlates with the total pore volume, but inversely with the surface area. As evidence, the BET surface area of SnO_2 and $Ni/SO_4/SnO_2$ solids is 43.5 and 134.2 m^2/g, respectively. Meanwhile, the total pore volume of SnO_2 and $Ni/SO_4/SnO_2$ solids has been measured at 0.16 and 0.11 cm^3/g, respectively. This observation was consistent with the findings investigated by Khalaf *et al.* (2011), Alaya & Rabah (2017), and Pradana *et al.* (2025b).

3.1.6 Bronsted Acidity

The results of *Bronsted* acidity test for TO and STO materials are summarized in Table 3. Initially, the acidity of TO solids were observed at 0.20 $mmol.g^{-1}$. In this condition, the number of acid sites was quantified at 4.1×10^{-3} $mmol.m^{-2}$. These values were comparable to other prior studies. Khalaf *et al.* (2011) reported the acid amount of tin oxide ($T_{calcine}$ = 600°C) at 0.11 $mmol.g^{-1}$. Khder *et al.* (2008) measured the acid sites number of tin oxide ($T_{calcine}$ = 550°C) at 0.35 $mmol.g^{-1}$. Moreover, tin oxide synthesized by Pradana *et al.* (2025b) through a hydrolysis method ($T_{calcine}$ = 500°C) showed a *Bronsted* acid amount of 0.19 $mmol.g^{-1}$.

Subsequently, sulfate modification provided an impressive addition of acid amount attached on the solid exterior. The total acidity of STO solids was detected at 2.03 $mmol.g^{-1}$. In other words, the acid amount in STO solids increased tenfold in comparison to TO solids. These findings emphasized that the elevation of SO_3 content in the STO, as XRF analysis results in Table 1, led to higher acid concentration. This acidity value was more excellent than other previous studies. Khder *et al.* (2008) and Khalaf *et al.* (2011) prepared STO catalysts with acid sites number of 1.30 and 0.40 $mmol.g^{-1}$, respectively. Pradana *et al.* (2025b) manufactured STO catalyst with hydrolysis tin(IV) chloride salt with acidity value of 1.15 $mmol.g^{-1}$. Alaya & Rabah (2017) outlined the acidity amount of sulfated-tungstated tin oxide ($T_{calcine}$ = 400°C) at 0.97 $mmol.g^{-1}$.

3.2 Evaluation of Isomerization Reaction

3.2.1 Biodiesel Component Observation

The results of GC-MS analysis for biodiesel feedstock and STO-catalyzed isomerization product are visualized in Fig. 7. According to these graphs, STO catalyst was established to catalyze skeletal and geometric isomerization. For skeletal isomerization, methyl iso-palmitate (Fig. 7c) and iso-stearate (Fig. 7e) as isomerized fatty esters were slightly detected in the

Table 3
Bronsted acidity of TO and STO materials.

Parameter	TO	STO
Bronsted acidity ($mmol.g^{-1}$)	0.20	2.03
Number of *Bronsted* acid sites ($mmol.m^{-2}$)	4.6×10^{-3}	1.5×10^{-2}

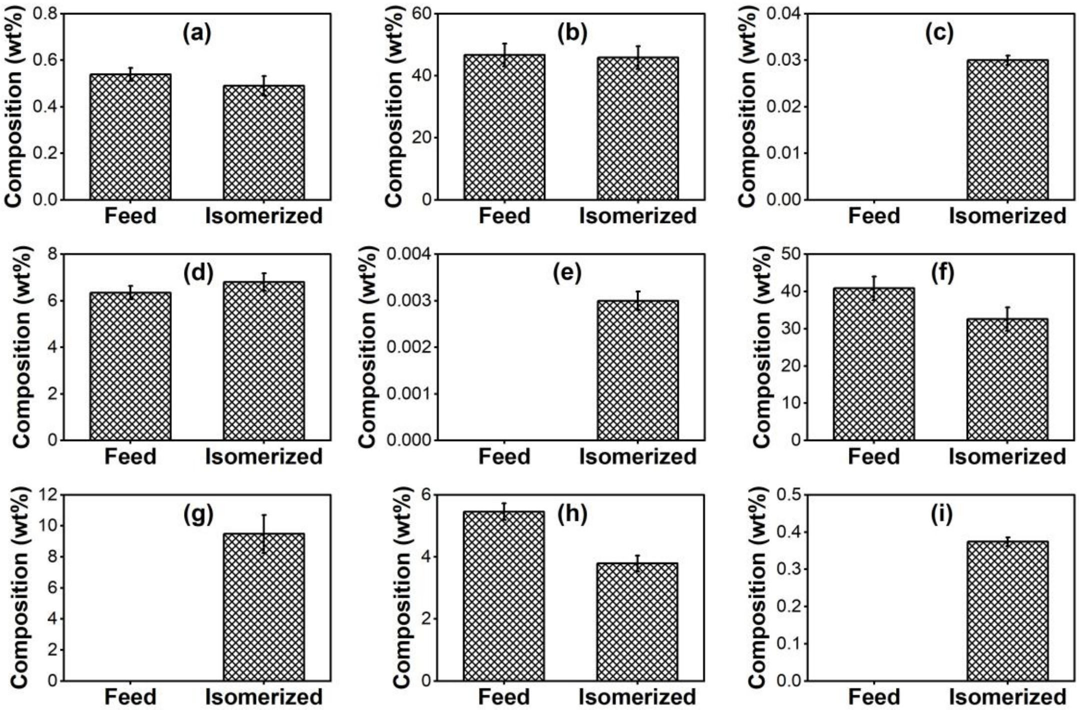

Fig. 7. Composition of biodiesel feedstock and STO-catalyzed isomerization product: (a) methyl myristate (C14:0); (b) methyl palmitate (C16:0); (c) methyl iso-palmitate (C16:0-iso); (d) methyl stearate (C18:0); (e) methyl iso-stearate (C18:0-iso); (f) methyl oleate (C18:1-*cis*); (g) methyl elaidate (C18:1-*trans*); (h) methyl linoleate (C18:2); and (i) palmitic acid.

reaction product. The composition of both components denoted values of 0.03±0.001 and 0.003±0.0002 wt%, respectively. Meanwhile, geometric or *cis-trans* isomerization was identified from the appearance of methyl elaidate (Fig. 7g) with a composition of 9.48±1.22 wt% in the biodiesel product. As mentioned in Fig. 2, methyl elaidate (*trans* structure) is a geometric isomer of methyl oleate (*cis* structure).

In addition to facilitating isomerization, STO catalyst also encouraged hydrogenation, hydrolysis, and cracking reactions. Hydrogenation reaction was primary indicated by the reduction of methyl linoleate (Fig. 7h) and the increase of methyl stearate (Fig. 7d). Additionally, the elevation in methyl oleate composition (Fig. 7f), after being reduced by *cis-trans* isomerization, provided compelling evidence for the occurrence of hydrogenation reaction. Later, hydrolysis was designated by the presence of palmitic acid (Fig. 7i) in the biodiesel product. It was generated from the reaction between methyl palmitate and residual water.

Lastly, cracking reaction was associated with an alleviation in the composition of methyl myristate (Fig. 7a) and palmitate (Fig. 7b). The decrease of methyl palmitate was attributed to this reaction because it was higher than the isomerized one. This reaction potentially produced shorter chain esters and gaseous-state hydrocarbons (Indarto *et al.,* 2006; Indarto, 2012). Based on this phenomenon, hydrogen was most likely derived from these hydrocarbons for fatty ester hydrogenation, promoting double- or triple-bond hydrocarbons.

3.2.2 Catalyst Activity Evaluation

Furthermore, the GC–MS analysis results were used as the basis for evaluating the reactivity of STO catalyst in the biodiesel isomerization. The calculation results of STO catalyst activity are tabulated in Table 4. Conversion ratio of overall reaction was quantified at 12.54±0.60%. In this condition, yields of skeletal and geometric isomerization were reported at 0.03±0.001 and 9.48±1.21%, respectively. The selectivity values for both isomerization schemes were counted at 0.26±0.02 and 75.66±5.77%. Totally, STO catalyst directed isomerization reaction with a selectivity of 75.92±5.79%. Hereafter, the side reactions of hydrogenation, hydrolysis, and cracking were documented with yields of 2.12±0.65, 0.37±0.01, and

Table 4
Conversion ratio, product yield, selectivity, and turnover frequency of STO-catalyzed reaction.

Parameter	Value
Conversion ratio (%)	12.54±0.60
Yield (%):	
Skeletal (branching) isomerization	0.03±0.001
Geometric (*cis-trans*) isomerization	9.48±1.21
Hydrogenation	2.12±0.65
Hydrolysis	0.37±0.01
Cracking	0.53±0.05
Selectivity (%):	
Skeletal (branching) isomerization	0.26±0.02
Geometric (*cis-trans*) isomerization	75.66±5.77
Hydrogenation	16.93±6.29
Hydrolysis	2.99±0.25
Cracking	4.20±0.16
Turnover frequency (h^{-1}):	
Overall	$1.75\times10^{-1}\pm8.5\times10^{-3}$
Skeletal (branching) isomerization	$5.02\times10^{-4}\pm1.8\times10^{-5}$
Geometric (*cis-trans*) isomerization	$1.31\times10^{-1}\pm1.7\times10^{-2}$
Hydrogenation	$2.95\times10^{-2}\pm8.9\times10^{-3}$
Hydrolysis	$6.00\times10^{-3}\pm1.9\times10^{-4}$
Cracking	$7.73\times10^{-3}\pm7.5\times10^{-4}$

0.53±0.05%, respectively. These undesirable reactions interfered the selectivity of STO catalyst by 24.13±6.71%.

Previous isomerization research using acid-based catalysts demonstrated various catalytic activities. Busto *et al.* (2012) isomerized n-hexadecane using $Pt/WO_3/ZrO_2$ and $Pt/SO_4/ZrO_2$ with isomer product yields of 4.1 and 0.2%, respectively. The work by Zhang *et al.* (2001) revealed the branching-reaction results of straight-chain cetane over nickel-doped WO_3/ZrO_2, achieving a maximum yield of 31.7%. Zhang *et al.* (2003) investigated sulfated zirconia catalyst for methyl oleate isomerization with a yield of 36%. Pradana *et al.* (2025b) presented catalytic performance of $Fe/SO_4/SnO_2$ catalyst for palm biodiesel isomerization with a selectivity of 90.8%. Liu *et al.* (2019) conducted isomerization of high oleic FAME using *p*-toluenesulfinic acid catalyst with the highest isomer selectivity of 79.8%.

In comparison with earlier studies, the catalyst performance in this work was still relatively low, despite the catalyst exhibiting high acidity and a large specific surface area. The most probable explanation is the presence of mass transfer limitations, which hinder the diffusion of reactant molecules from the bulk liquid to the acid sites on the catalyst pore surface. Then, this resistance is likely triggered by the relatively small pore size, which restricts the continuous diffusion of reactant and product molecules. The average pore diameter of the catalyst was measured to be 3.2 nm. In comparison, the size of a representative fatty ester molecule in palm biodiesel (methyl stearate) is approximately 2.45 nm (Anwar & Garforth, 2016). Based on these data, the reactant and product molecules are able to access and diffuse through the catalyst pores. However, the pore size does not allow the simultaneous transport of two or more molecules, thereby giving rise to the resistance of internal pore mass transfer.

This observation was further supported by the analysis of the acid site activity using turnover frequency (TOF) parameter. The TOF of overall reaction was calculated to be $1.75\times10^{-1}\pm8.5\times10^{-3}$ h^{-1}. The highest acid site activity was observed for the *cis–trans* isomerization reaction, with a TOF of $1.31\times10^{-1}\pm1.7\times10^{-2}$ h^{-1}. In other words, approximately 75% of the acid site activity was associated with promoting the formation of methyl elaidate from methyl oleate. This value is relatively low compared with that of Ni/ZSM-22 catalysts (TOF = 9.4–14.2 h^{-1}) for the hydroisomerization of long-chain fatty acids (Yan *et al.*, 2025), as well as SAPO-11 (TOF = 8.3 h^{-1}) and ZSM-35 (TOF = 14.8 h^{-1}) for n-hexadecene isomerization (Bruno & Dooley, 2015). Subsequently, a number of related catalysts demonstrate comparable TOF values to that investigated in this work, including Pt/β-zeolite (TOF < 0.5 h^{-1}) for n-hexane isomerization (Wang et al., 2024), and Ru/Al_2O_3 (TOF = 0.22–0.77 h^{-1}) for linoleic acid isomerization (Bernas *et al.*, 2004). Meanwhile, several other catalysts have lower TOF values than those of this examined catalyst, such as $Pd\text{-}Mg/SiO_2$ (TOF = 1.1×10^{-2} h^{-1}) for the hydroisomerization of soybean biodiesel (Thunyaratchatanon *et al.*, 2016) and SO_4/SnO_2 (TOF = 1.76×10^{-2} h^{-1}) prepared via hydrolysis method (Pradana *et al.*, 2025).

3.2.3 Cold Flow Properties Measurement

A summary of the experimental results and reference standards of biodiesel cold flow properties is provided in Table 5. According to the measurements, the isomerized biodiesel was found to have a PP of 11°C and a CP of 16.1±0.05°C. This PP value was slightly lower than that of the feedstock (ΔPP = –1°C). This value fails to comply with the PP standard defined in ASTM-D6751. However, institutions that implement European standard for biodiesel, along with additional requirement fulfilment, will find it to be a manageable challenge.

Table 5
Cold flow properties of biodiesel feedstock, product, and standards.

Biodiesel	PP (°C)	CP (°C)
Feedstock	12	15.60±0.10
Isomerization product	11	16.10±0.05
ASTM Standard (D-6751)*)	min. –15 max. 10	min. –3 max. 12
EU Standard (EN-14214)*)	–	–

Source: *) Pradana *et al.*, 2024

Thereafter, CP value of the isomerized biodiesel revealed an increase of 0.50±0.15°C from the feedstock (ΔCP = 0.50±0.15°C). It implied that geometric isomerization, as a dominant reaction, slightly deteriorated biodiesel cold flow properties. These findings aligned with the fundamental theory explained by Anwar & Garforth (2016), indicating that *trans*-structured fatty esters worsened biodiesel cold fluidity. The reduction in cold flow properties was also attributed to the elevation of biodiesel saturation degree, as visualized in Fig. 2. This observation was reflected by an alleviation in methyl linoleate (poly-double-bond fatty ester) accompanied by an escalation in the total content of mono-unsaturated fatty esters (methyl oleate and methyl elaidate). In addition, the slight escalation in CP was also contributed by the higher level of methyl stearate in the biodiesel product.

Then, for skeletal isomer products, they exerted a negligible improvement effect on the biodiesel cold flow properties due to their very low concentrations. Moreover, their other physicochemical properties, including density, kinematic viscosity, cetane number, and oxidation stability, differ only marginally from those of their corresponding straight-chain fatty esters (Pradana *et al.*, 2024; Sierra-Cantor & Guerrero-Fajardo, 2017). According to the absolute values of PP (11°C) and CP (16.10±0.05°C), the isomerized biodiesel does not comply with ASTM standard (D6751). Nonetheless, this biodiesel product can be applied in areas that adhere to European standards, with the responsibility of reporting cold flow properties.

3.2.4 Oxidation Stability Investigation

The investigation results and standards of biodiesel oxidation stability are tabulated in Table 6. This oxidation analysis indicated that the induction period for biodiesel product was 19.38 h. This value was higher than the feedstock (18.02 h). The findings implied that geometric isomerization demonstrated the enhancement of biodiesel oxidation stability. As discussed by Anwar & Garforth (2016), methyl elaidate (OS = 7.7 h) exhibits significantly higher oxidation stability than methyl oleate (OS = 2.5 h). Moreover, these results were also attributed to the reduced composition of poly-unsaturated methyl linoleate and the increased fraction of mono-unsaturated fatty esters, as illustrated in Fig. 2. This condition led to a higher degree of saturation in the biodiesel product, translating into enhanced oxidation stability. Meanwhile, skeletal isomer products derived from saturated fatty esters exhibit oxidation stability comparable to that of their parent components, since the degree of saturation is not modified. Additionally, due to their relatively minor composition, the effect of these components was negligible in this study.

According to several standards issued by ASTM, European Committee for Standardization, and Indonesian Government,

Table 6
Oxidation stability of biodiesel isomerization samples and international standards.

Biodiesel	OS (h)
Feedstock	18.02
Isomerization product	19.38
ASTM Standard (D-6751)*)	min. 3
EU Standard (EN-14214)*)	min. 8

Source: *) Pradana *et al.*, 2024

the stability of biodiesel product against oxidation satisfies with these established regulations. The observation by Liu *et al.* (2019) elucidated that geometric isomerization affected the oxidative resistance of biodiesel. The improvement of oxidation stability for camelia seed, safflower seed, and sunflower FAMEs was pointed at 3.3, 0.2, and 5.6 h, respectively. Meanwhile, the other STO-catalyzed isomerization, conducted by Pradana *et al.* (2025b), presented the improvement of biodiesel oxidation stability at 1.6 h.

3.3 Investigation of Bio-additives Insertion

3.3.1 Effect on Cold Flow Properties

The measurement data of cold flow properties for biodiesel with bio-additive insertion are presented in Table 7. The first evaluated bio-additives was turpentine oil. The insertion of 1 vol% turpentine oil in biodiesel did not have any effect on the pour point alteration. Then, the addition of this bio-additive at percentages of 3 and 5 vol% slightly diminished the PP by 1°C (ΔPP = −1°C). While, the mixing of biodiesel and 10 vol% turpentine oil led to a decrease in the pour point by 2°C. Later, the inclusion of turpentine oil at concentrations of 1−10 vol% progressively reduced the mean pour point from 0.40±0.10 to 1.90±0.20°C.

Thereafter, the second observed bio-additive was α-terpineol. The effect of α-terpineol addition on biodiesel PP was similar to turpentine oil. However, the introduction of this bio-additive provided greater leverage on alleviating biodiesel CP than turpentine oil. The reduction in the average biodiesel CP at α-terpineol percentages of 1, 3, 5, and 10 vol% was recorded at 0.40±0.20, 1.05±0.15, 1.75±0.15, and 2.50±0.20°C, respectively. These findings signify that α-terpineol has potential as a cold flow properties improver for biodiesel, in addition to being an octane booster for gasoline (Vallinayagam *et al.*, 2017). Nevertheless, it requires further study to ensure the compliance of biodiesel products with international standards (Table 5).

For comparison, Achmad *et al.* (2025) investigated the effect of 5 and 10 vol% turpentine oil on the CP of B40 fuel with a decline of ±0.45 and ±0.90°C, respectively. Zhang *et al.* (2022) proposed the grafted copolymer poly-tetradecyl methacrylate-styrene-citric anhydride (PTM-St-CA), at concentrations up to 2 wt%, to improve low-temperature operability of diesel-FAMEs blending fuel with the best depressive impacts on PP and CP of ±12.5°C and ±3.7°C, respectively. In the research conducted by Senra *et al.* (2019), introducing additives from glycerol derivatives at 15 wt% into FAMEs yielded the highest CP reduction of 3.6°C.

Table 7
Cold flow properties of biodiesel feedstock and products with bio-additive introduction.

Biodiesel	PP (°C)	CP (°C)
Feedstock	9	14.00±0.10
Products with:		
A. turpentine oil introduction		
(1) 1 vol%	9	13.60±0.00
(2) 3 vol%	8	13.40±0.10
(3) 5 vol%	8	13.20±0.10
(4) 10 vol%	7	12.10±0.10
B. α-terpineol introduction		
(1) 1 vol%	9	13.60±0.10
(2) 3 vol%	8	12.95±0.05
(3) 5 vol%	8	12.25±0.05
(4) 10 vol%	7	11.50±0.10

3.3.2 Effect on Oxidation Stability

Table 8 presents the oxidation stability results of biodiesel containing bio-additives. Generally, the incorporation of turpentine oil and α-terpineol negatively affected the OS of biodiesel. For the first bio-derived additives, the insertion of turpentine oil to biodiesel at levels of 1, 3, 5, and 10 vol% alleviated the OS by 2.89, 7.56, 21.31, and 21.32 h, respectively. It revealed that the utilization of turpentine oil as a biodiesel additive should remain below 5 vol% to avoid significant reduction in OS and comply this property with international standards (Table 6).

Meanwhile, the inclusion of α-terpineol, at the same percentages, exhibited a lower reduction in OS properties than that of turpentine oil. The application of α-terpineol at a percentage of 5 vol% or below is still permitted, as its oxidation stability exceeds the threshold of international standards. Nonetheless, this biodiesel product cannot be implemented in several countries or regions that require higher OS, including Indonesia (OS ≥ 11 h) and Brazil (OS ≥ 13 h).

Compared to prior studies, Nambiraj & Kumar (2024) inserted the natural extract from *Citrus Aurantifolia* L to extend biodiesel storage time from 2.64 to 11.2 h. Zhang *et al.* (2022) incorporated copolymer PTM-St-CA to refine oxidation stability of soybean-biodiesel blending fuel from 1.6 to 8.7 h. Later, in the study by Achmad *et al.* (2025), the addition of turpentine oil adversely influenced the oxidation stability of B40 blending fuel. The introduction of 5 vol% turpentine oil diminished biodiesel stability against oxidation from 311 to 250 min.

Table 8
Oxidation stability of biodiesel feedstock and products with bio-additives introduction.

Biodiesel	OS (h)
Feedstock	21.36
Products with:	
A. turpentine oil introduction	
(1) 1 vol%	18.47
(2) 3 vol%	13.80
(3) 5 vol%	0.05
(4) 10 vol%	0.04
B. α-terpineol introduction	
(1) 1 vol%	23.02
(2) 3 vol%	16.51
(3) 5 vol%	10.36
(4) 10 vol%	3.71

4. Conclusion

The process of isomerizing palm biodiesel was proven to perform with STO catalyst, although the reaction conversion was still relatively low at 12.54±0.60%. In this condition, the TOF of overall reaction and the selectivity of isomerization were quantified at $1.75\times10^{-1}\pm8.5\times10^{-3}$ h^{-1} and 75.92±5.79%, respectively. The most obtrusive process was geometric (*cis-trans*) isomerization, transforming methyl oleate into methyl elaidate. This reaction contributed to the decline in PP (ΔPP = –1°C), the slight elevation in CP (ΔCP = 0.50±0.15°C), and the prolongation of OS (ΔOS = 1.36 h). For bio-additive insertion, the optimum result was the addition of α-terpineol at concentration of 5 vol%. This condition provided better cold flow properties (ΔPP = –1°C and ΔCP = –1.75±0.15°C) than the isomerization process. Nevertheless, it significantly alleviated the OS of biodiesel (ΔOS = –11 h), although the absolute value (OS = 10.36 h) still complies with the international standards ASTM D6751 and EN 14214.

Acknowledgments

The authors gratefully acknowledge the assistance of Candra Egiyawati and Sefira Nur Amalia during the isomerization experiments.

Author Contributions: A.I.: conceptualization, methodology, formal analysis, validation, writing—original draft, writing—review and editing, supervision, Y.S.P: Conceptualization, methodology, investigation, formal analysis, validation, data curation, visualization, writing—original draft, writing—review and editing, A.K.A.: investigation, I.G.B.N.M.: conceptualization, methodology, formal analysis, validation, supervision, T.P.: conceptualization, methodology, formal analysis, validation, supervision, T.H.S.: conceptualization, methodology, validation. All authors have read and agreed to the published version of the manuscript.

Funding: Financial support for this study was provided by Center for Higher Education funding and Assessment (PPAPT), Ministry of Higher Education, Science, and Technology of the Republic of Indonesia through Indonesia Education Scholarship (BPI) Program under Grant No. 01198/BPPT/BPI.06/9/2023. This research was also partially funded by the Indonesian Endowment Fund for Education Agency (LPDP) on behalf of Ministry of Higher Education, Science, and Technology of the Republic of Indonesia and managed under the EQUITY Program (Grant No. 4298/B3/DT.03.08/2025). Several analytical testing in this research was supported by additional funding from The Asahi Glass Foundation via Overseas Research Grant 2025 under Grant No. 4274a/IT1.C07.2/TA.00/2025.

Conflicts of Interest: The authors declare no conflict of interest.

References

Achmad, A. K. F., Fathurrahman, N. A., Kunarti, E. S., Wibowo, C. S., Khalil, M., & Al-Saadi, A. A. (2025). Optimizing cold-flow properties and oxidation stability of B40 biodiesel blend with turpentine oil and ethanol: Experimental and quantum chemical approach. *Fuel*, 381, 133258. https://doi.org/10.1016/j.fuel.2024.133258

Akkera, H. S., Mann, V., Varalakshmi, B. N., Ploloju, M., Kambhala, N., & Venkatesh, G. (2023). Effect of Sr-doped on physical and photoluminescence properties of SnO_2 transparent conducting oxide thin films. *Journal of Materials Science: Materials in Electronics*, 34(12), 1044. https://doi.org/10.1007/s10854-023-10473-z

Alaya, M. N., & Rabah, M. A. (2017). Some physico-chemical properties and catalytic activity of sulfate ion supported on WO_3/SnO_2 catalyst. *Arabian Journal of Chemistry*, 10, S439–S449. https://doi.org/10.1016/j.arabjc.2012.10.004

Amran, N. A., Bello, U., & Hazwan Ruslan, M. S. (2022). The role of antioxidants in improving biodiesel's oxidative stability, poor cold flow properties, and the effects of the duo on engine performance: A review. *Heliyon*, 8(7), e09846. https://doi.org/10.1016/j.heliyon.2022.e09846

Anwar, A., & Garforth, A. (2016). Challenges and opportunities of enhancing cold flow properties of biodiesel via heterogeneous catalysis. *Fuel*, 173, 189–208. https://doi.org/10.1016/j.fuel.2016.01.050

Arata, K., Matsuhashi, H., Hino, M., & Nakamura, H. (2003). Synthesis of solid superacids and their activities for reactions of alkanes. *Catalysis Today*, 81(1), 17–30. https://doi.org/10.1016/S0920-5861(03)00098-1

Ballesteros, R., García, D., Bustamante, F., Alarcón, E., & Lapuerta, M. (2020). Oxyfunctionalized turpentine: Evaluation of properties as automotive fuel. *Renewable Energy*, 162, 2210–2219. https://doi.org/10.1016/j.renene.2020.10.026

Bernas, A., Kumar, N., Laukkanen, P., Väyrynen, J., Salmi, T., & Murzin, D. Y. (2004). Influence of ruthenium precursor on catalytic activity of Ru/Al2O3 catalyst in selective isomerization of linoleic acid to cis-9,trans-11- and trans-10,cis-12-conjugated linoleic acid. *Applied Catalysis A: General*, 267(1–2), 121–133. https://doi.org/10.1016/j.apcata.2004.02.032

Bruno, J. E., & Dooley, K. M. (2015). Double-bond isomerization of hexadecenes with solid acid catalysts. *Applied Catalysis A: General*, 497, 176–183. https://doi.org/10.1016/j.apcata.2015.03.009

Busto, M., Dosso, L. A., Vera, C. R., & Grau, J. M. (2012). Composite catalysts of Pt/SO42-ZrO2 and Pt/WO_3-ZrO_2 for producing high octane isomerizate by isomerization-cracking of long paraffins. *Fuel Processing Technology*, 104, 128–135. https://doi.org/10.1016/j.fuproc.2012.04.040

Dey, S., Reang, N. M., Das, P. K., & Deb, M. (2021). A comprehensive study on prospects of economy, environment, and efficiency of palm oil biodiesel as a renewable fuel. *Journal of Cleaner Production*, 286, 124981. https://doi.org/10.1016/j.jclepro.2020.124981

Hino, M., Takasaki, S., Furuta, S., Matsuhashi, H., & Arata, K. (2007). meta-Stannic acid as an effective support for the preparation of sulfated and tungstated stannias. *Applied Catalysis A: General*, 321(2), 147–154. https://doi.org/10.1016/j.apcata.2007.01.044

Indarto, A., Choi, J. W., Lee, H., Song, H. K. (2006). Treatment of CCl_4 and $CHCl_3$ emission in a gliding-arc plasma. *Plasma Devices and Operations*, 14(1), 1-14. https://doi.org/10.1080/10519990500493833

Indarto, A. (2012). Decomposition of dichlorobenzene in a dielectric barrier discharge. *Environmental Technology*, 33(6), 663-666. https://doi.org/10.1080/09593330.2011.587026

Jhoni, F. A. M., & Pradana, Y. S. (2025). Bio-crude oil production from microalgae Nannochloropsis sp. via non-catalytic hydrothermal liquefaction. *AIP Conference Proceedings*, 3295, 040003. https://doi.org/10.1063/5.0269836

Khalaf, H. A., Mansour, S. E., & El-Madani, E. A. (2011). The influence of sulfate contents on the surface properties of sulfate-modified tin(IV) oxide catalysts. *Journal of the Association of Arab Universities for Basic and Applied Sciences*, 10(1), 15–20. https://doi.org/10.1016/j.jaubas.2011.06.003

Khder, A. S., El-Sharkawy, E. A., El-Hakam, S. A., & Ahmed, A. I. (2008). Surface characterization and catalytic activity of sulfated tin oxide catalyst. *Catalysis Communications*, 9(5), 769–777. https://doi.org/10.1016/j.catcom.2007.08.022

Knothe, G., & Dunn, R. O. (2009). A Comprehensive Evaluation of the Melting Points of Fatty Acids and Esters Determined by Differential Scanning Calorimetry. *Journal of the American Oil Chemists' Society*, 86(9), 843–856. https://doi.org/10.1007/s11746-009-1423-2

Lanjekar, R. D., & Deshmukh, D. (2016). A review of the effect of the composition of biodiesel on NO_x emission, oxidative stability and cold flow properties. *Renewable and Sustainable Energy Reviews*, 54, 1401–1411. https://doi.org/10.1016/j.rser.2015.10.034

László, T. (2023). Ambivalent changes in the correlation of energy consumption and economic growth in the member states of the European Union (2010–2019). *Heliyon*, 9(3), e14550. https://doi.org/10.1016/j.heliyon.2023.e14550

Leng, L., Li, W., Li, H., Jiang, S., & Zhou, W. (2020). Cold Flow Properties of Biodiesel and the Improvement Methods: A Review. *Energy & Fuels*, 34(9), 10364–10383. https://doi.org/10.1021/acs.energyfuels.0c01912

Liu, A., Zhu, M., & Dai, B. (2019). A novel high-performance SnO_2 catalyst for oxidative desulfurization under mild conditions. *Applied Catalysis A: General*, 583, 117134. https://doi.org/10.1016/j.apcata.2019.117134

Liu, W., Lu, G., Yang, G., & Bi, Y. (2019). Improving oxidative stability of biodiesel by cis-trans isomerization of carbon-carbon double bonds in unsaturated fatty acid methyl esters. *Fuel*, 242, 133–139. https://doi.org/10.1016/j.fuel.2018.12.132

Lugito, G., Pamungkas, A. Y., Realdi, M. N. D., Alam, A. K., Egiyawati, C., Pradana, Y. S., Adhi, T. P., Soerawidjaja, T. H., Makertihartha, I. G. B. N., Mohtar, W. H. M. W., Kurnia, I., & Indarto, A. (2025). Biodiesel Stability Enhancement Through Catalytic Transfer Hydrogenation Using Glycerol as Hydrogen Donor. *Eng*, 6(5), 94. https://doi.org/10.3390/eng6050094

Maghrebi, R., Buffi, M., Bondioli, P., & Chiaramonti, D. (2021). Isomerization of long-chain fatty acids and long-chain hydrocarbons: A review. *Renewable and Sustainable Energy Reviews*, 149, 111264. https://doi.org/10.1016/j.rser.2021.111264

Misra, P., Alvarez-Majmutov, A., & Chen, J. (2023). Isomerization catalysts and technologies for biorefining: Opportunities for producing sustainable aviation fuels. *Fuel*, 351, 128994. https://doi.org/10.1016/j.fuel.2023.128994

Moser, B. R. (2009). Comparative oxidative stability of fatty acid alkyl esters by accelerated methods. *JAOCS, Journal of the American Oil Chemists' Society*, 86(7), 699–706. https://doi.org/10.1007/s11746-009-1376-5

Nambiraj, M., & Suresh, K. (2024). Exploring the role of natural antioxidant additives extracted from agro wastes in prolonging biodiesel's storage stability. *Industrial Crops and Products*, 212, 118321. https://doi.org/10.1016/j.indcrop.2024.118321

OECD, & FAO. (2024a) *OECD Agriculture Statistics (database)*. https://data-explorer.oecd.org/. Accessed on 6 January 2025

OECD, & FAO. (2024b) *OECD-FAO Agricultural Outlook 2024-2033*. OECD Publishing, Paris and Rome. https://doi.org/10.1787/4c5d2cfb-en

Pan, H., Xia, Q., Wang, Y., Shen, Z., Huang, H., Ge, Z., Li, X., He, J., Wang, X., Li, L., & Wang, Y. (2022). Recent advances in biodiesel production using functional carbon materials as acid/base catalysts. *Fuel Processing Technology*, 237, 107421. https://doi.org/10.1016/j.fuproc.2022.107421

Pradana, Y. S., Azmi, F. A., Masruri, W., & Hartono, M. (2018). Biodiesel Production from Wet Spirulina sp. by One-Step Extraction-Transesterification. *MATEC Web of Conferences*, 156, 03009. https://doi.org/10.1051/matecconf/201815603009

Pradana, Y. S., Dewi, R. N., Di Livia, K., Arisa, F., Rochmadi, Cahyono, R. B., & Budiman, A. (2020). Advancing biodiesel production from microalgae Spirulina sp. By a simultaneous extraction-transesterification process using palm oil as a co-solvent of methanol. *Open Chemistry*, 18(1), 833–842. https://doi.org/10.1515/chem-2020-0133

Pradana, Y. S., Makertihartha, I. G. B. N., Indarto, A., & Prakoso, T. (2025a). Biodiesel production from palm oil using potassium-loaded carbon as a heterogeneous catalyst: Kinetic study and process modification analysis. *AIP Conference Proceedings*, 3295, 040012. https://doi.org/10.1063/5.0272306

Pradana, Y. S., Makertihartha, I. G. B. N., Indarto, A., Prakoso, T., & Soerawidjaja, T. H. (2024). A Review of Biodiesel Cold Flow Properties and Its Improvement Methods: Towards Sustainable Biodiesel Application. *Energies*, 17(18), 4543. https://doi.org/10.3390/en17184543

Pradana, Y. S., Makertihartha, I. G. B. N., Prakoso, T., Soerawidjaja, T. H., & Indarto, A. (2025b). Biodiesel Isomerization Using Sulfated Tin(IV) Oxide as a Superacid Catalyst to Improve Cold Flow Properties. *Technologies*, 13(5), 203. https://doi.org/10.3390/technologies13050203

Pradana, Y. S., Sadewo, B. R., Haryanto, S. A., & Sudibyo, H. (2021). Selection of oil extraction process from *Chlorella* species of microalgae by using multi-criteria decision analysis technique for biodiesel production. *Open Chemistry*, 19(1), 1029–1042. https://doi.org/10.1515/chem-2021-0092

Prasakti, L., Pratama, S. H., Fauzi, A., Pradana, Y. S., & Budiman, A. (2020). Exergy analysis of conventional and hydrothermal liquefaction–esterification processes of microalgae for biodiesel production. *Open Chemistry*, 18(1), 874–881. https://doi.org/10.1515/chem-2020-0132

Riyadi, T. W. B., Spraggon, M., Herawan, S. G., Idris, M., Paristiawan, P. A., Putra, N. R., R, M. F., Silambarasan, R., & Veza, I. (2023). Biodiesel for HCCI engine: Prospects and challenges of sustainability biodiesel for energy transition. *Results in Engineering*, 17, 100916. https://doi.org/10.1016/j.rineng.2023.100916

Santos, S. M., Wolf-Maciel, M. R., & Fregolente, L. V. (2023). Cold flow properties: Applying exploratory analyses and assessing predictive methods for biodiesel and diesel-biodiesel blends. *Sustainable Energy Technologies and Assessments*, 57, 103220. https://doi.org/10.1016/j.seta.2023.103220

Senra, M., McCartney, S. N., & Soh, L. (2019). The effect of bio-derived additives on fatty acid methyl esters for improved biodiesel cold flow properties. *Fuel*, 242, 719–727. https://doi.org/10.1016/j.fuel.2019.01.086

Sia, C. B., Kansedo, J., Tan, Y. H., & Lee, K. T. (2020). Evaluation on biodiesel cold flow properties, oxidative stability and enhancement strategies: A review. *Biocatalysis and Agricultural Biotechnology*, 24, 101514. https://doi.org/10.1016/j.bcab.2020.101514

Sierra-Cantor, J. F., & Guerrero-Fajardo, C. A. (2017). Methods for improving the cold flow properties of biodiesel with high saturated fatty acids content: A review. *Renewable and Sustainable Energy Reviews*, 72, 774–790. https://doi.org/10.1016/j.rser.2017.01.077

Suzihaque, M. U. H., Alwi, H., Kalthum Ibrahim, U., Abdullah, S., & Haron, N. (2022). Biodiesel production from waste cooking oil: A brief review. *Materials Today: Proceedings*, 63, S490–S495. https://doi.org/10.1016/j.matpr.2022.04.527

Thommes, M., Kaneko, K., Neimark, A. V., Olivier, J. P., Rodriguez-Reinoso, F., Rouquerol, J., & Sing, K. S. W. (2015). Physisorption of gases, with special reference to the evaluation of surface area and pore size distribution (IUPAC Technical Report). *Pure and Applied Chemistry*, 87(9–10), 1051–1069. https://doi.org/10.1515/pac-2014-1117

Thunyaratchatanon, C., Jitjamnong, J., Luengnaruemitchai, A., Numwong, N., Chollacoop, N., & Yoshimura, Y. (2016). Influence of Mg modifier on cis-trans selectivity in partial hydrogenation of biodiesel using different metal types. *Applied Catalysis A: General*, 520, 170–177. https://doi.org/10.1016/j.apcata.2016.04.019

Thushari, I., Babel, S., & Samart, C. (2019). Biodiesel production in an autoclave reactor using waste palm oil and coconut coir husk derived catalyst. *Renewable Energy*, 134, 125–134. https://doi.org/10.1016/j.renene.2018.11.030

Vallinayagam, R., Vedharaj, S., Naser, N., Roberts, W. L., Dibble, R. W., & Sarathy, S. M. (2017). Terpineol as a novel octane booster for extending the knock limit of gasoline. *Fuel*, 187, 9–15. https://doi.org/10.1016/j.fuel.2016.09.034

Varala, R., Narayana, V., Kulakarni, S. R., Khan, M., Alwarthan, A., & Adil, S. F. (2016). Sulfated tin oxide (STO) - Structural properties and application in catalysis: A review. *Arabian Journal of Chemistry*, 9(4), 550–573. https://doi.org/10.1016/j.arabjc.2016.02.015

Wahyono, Y., Hadiyanto, H., Budihardjo, M. A., & Adiansyah, J. S. (2020). Assessing the Environmental Performance of Palm Oil Biodiesel Production in Indonesia: A Life Cycle Assessment Approach. *Energies*, *13*(12), 3248. https://doi.org/10.3390/en13123248

Wang, L., Wang, H., Fan, J., & Han, Z. (2023). Synthesis, catalysts and enhancement technologies of biodiesel from oil feedstock – A review. *Science of The Total Environment*, 904, 166982. https://doi.org/10.1016/j.scitotenv.2023.166982

Wang, P., Chen, T., Qiu, Z., Yao, W., Liu, P., Zhang, Y., Song, Y., Cui, Q., & Bao, X. (2024). Pt-promoted mesoporous Beta zeolite catalysts for n-Hexane isomerization with enhanced selectivity to dibranched isomers. *Fuel*, 368, 131593. https://doi.org/10.1016/j.fuel.2024.131593

Wenxiang, F., Baosheng, D., Wei, W., Chenglin, Y., & Xueyuan, C. (2005). Manufacturing method of metastannic acid (tin dioxide) powder. *China National Intellectual Property Administration*, CN1657417A. https://patents.google.com/patent/CN1657417A/en

Yan, Z., Zhang, L., Shao, Y., Shu, Z., Huang, P., Fu, W., & Tang, T. (2025). Ni catalyst on nanocrystal ZSM-22 boosting the deoxygenation-hydroisomerization of fatty acid to long-chain iso-alkanes with remarkable isomerization selectivity. *Journal of Catalysis*, 449, 116234. https://doi.org/10.1016/j.jcat.2025.116234

Yu, K., Kumar, N., Aho, A., Roine, J., Heinmaa, I., Murzin, D. Y., & Ivaska, A. (2016). Determination of acid sites in porous aluminosilicate solid catalysts for aqueous phase reactions using potentiometric titration method. *Journal of Catalysis*, 335, 117–124. https://doi.org/10.1016/j.jcat.2015.12.010

Yuarrina, W. P., Pradana, Y. S., Budiman, A., Majid, A. I., Indarto, & Suyono, E. A. (2018). Study of cultivation and growth rate kinetic for mixed cultures of local microalgae as third generation (G-3) bioethanol feedstock in thin layer photobioreactor. *Journal of Physics: Conference Series*, 1022, 012051. https://doi.org/10.1088/1742-6596/1022/1/012051

Zhang, S., Zhang, Y., Tierney, J. W., & Wender, I. (2001). Anion-modified zirconia: effect of metal promotion and hydrogen reduction on hydroisomerization of n-hexadecane and Fischer-Tropsch waxes. *Fuel Processing Technology*, 69, 59–71. https://doi.org/10.1016/S0378-3820(00)00133-8

Zhang, S., Zhang, Z., & Steichen, D. (2003). Skeletal Isomerization of Alkyl Esters and Derivatives Prepared Therefrom. *Unites States Patent*, US20030191330A1. https://patents.google.com/patent/US20030191330A1/en

Zhang, X., Li, N., Wei, Z., Dai, B., & Han, S. (2022). Synthesis and evaluation of bifunctional polymeric agent for improving cold flow properties and oxidation stability of diesel-biodiesel blends. *Renewable Energy*, 196, 737–748. https://doi.org/10.1016/j.renene.2022.06.110